Front. Energy 2017, 11(3): 260–267
DOI 10.1007/s11708-017-0499-x

RESEARCH ARTICLE

Hongjie ZHANG, Yachao ZENG, Longsheng CAO, Limeng YANG, Dahui FANG, Baolian YI, Zhigang SHAO

Enhanced electrocatalytic performance of ultrathin PtNi alloy nanowires for oxygen reduction reaction

Abstract In this paper, ultrathin Pt nanowires (Pt NWs) and PtNi alloy nanowires (PtNi NWs) supported on carbon were synthesized as electrocatalysts for oxygen reduction reaction (ORR). Pt and PtNi NWs catalysts composed of interconnected nanoparticles were prepared by using a soft template method with CTAB as the surface active agent. The physical characterization and electrocatalytic performance of Pt NWs and PtNi NWs catalysts for ORR were investigated and the results were compared with the commercial Pt/C catalyst. The atomic ratio of Pt and Ni in PtNi alloy was approximately 3 to 1. The results show that after alloying with Ni, the binding energy of Pt shifts to higher values, indicating the change of its electronic structure, and that Pt_3Ni NWs catalyst has a significantly higher electrocatalytic activity and good stability for ORR as compared to Pt NWs and even Pt/C catalyst. The enhanced electrocatalytic activity of Pt_3Ni NWs catalyst is mainly resulted from the downshifted-band center of Pt caused by the interaction between Pt and Ni in the alloy, which facilitates the desorption of oxygen containing species (O_{ads} or OH_{ads}) and the release of active sites.

Keywords PtNi alloy, nanowires, oxygen reduction reaction, enhanced activity, good stability

1 Introduction

The proton exchange membrane fuel cell (PEMFC) with the advantages of high energy conversion efficiency, totally environmentally friendliness and the renewal of hydrogen resources has attracted wide attention and research interests for promising clean power sources [1,2]. To realize energy conversion, the oxygen reduction reaction (ORR) at the cathode is one of the most important processes and one of the biggest problems to be solved because of the sluggish ORR kinetics, the scarcity and high cost of Pt which is used as ORR catalyst [3–5]. Therefore, attempts to lower the Pt loading without damage or even with enhancement to the catalytic activity of the catalysts, i.e., to improve the effective utilization of Pt is of great significance. Generally, there are two different approaches or strategies to reduce the cost of the catalyst. One is developing non-noble metallic catalysts instead of Pt-based materials for ORR, which however has achieved neither catalytic activity nor stability to the same level as Pt catalysts under the operating conditions of PEMFC [6–8]. The other one is that taking advantage of the beneficial tuning of Pt electronic properties via the interaction between Pt and other transition metals in PtM alloys or Pt based core-shell catalysts to substantially improve the electrocatalytic activity and reduce the amount of precious metals [5,9–12].

In fact, many encouraging research results about Pt-based catalysts are obtained. For example, the incorporation of transition metals of Fe, Co, Ni, and Cu etc. into Pt nanostructures is proved to be an effective strategy to enhance the electrocatalytic activity of Pt for ORR [13–16]. Pure Pt catalysts appear to over bind the intermediate species on their surfaces emerged from the fuel cell operation process [17]. Therefore, the over binding adsorbates will lead to a shortage of active sites and a decrease of catalytic activity. Among wide range of compositions, the PtNi bimetallic materials, for example, different nanostructured Pt_3Ni alloys have made the most significant progress in improving the activity [18–20]. The

Received Jul. 11, 2017; accepted Jul. 20, 2017; online Aug. 25, 2017

Hongjie ZHANG, Yachao ZENG, Longsheng CAO, Limeng YANG, Dahui FANG
Fuel Cell System and Engineering Laboratory, Dalian Institute of Chemical Physics, Chinese Academy of Sciences, Dalian 116023, China; University of the Chinese Academy of Sciences, Beijing 100039, China

Baolian YI, Zhigang SHAO (✉)
Fuel Cell System and Engineering Laboratory, Dalian Institute of Chemical Physics, Chinese Academy of Sciences, Dalian 116023, China
E-mail: zhgshao@dicp.ac.cn

electronic effect and strain effect produced by electron-electron interaction and lattice contraction which finally resulted in the downshift of d-band center in the bimetallic structures are believed to be the contributions to the improvement of activity [21]. Other than composition, the effect of structure is not negligible. Pt alloy nanoparticles supported on carbon typically suffer from inadequate stability because of the dissolution or Ostwald agglomeration of the particles. In contrast, multi-dimensional nanostructures such as nanotubes or nanoframes should have much better durability because of the inherent structural stability.

Herein, a facile synthesis of ultrathin Pt and PtNi alloy nanowires with controlled composition (nearly 3:1 for Pt: Ni) and their application as the electrocatalyst for ORR is reported. The nanowires are composed of interconnected nanoparticles prepared by using a soft template method with CTAB as the surface active agent and $NaBH_4$ as the reductant. The physical characterization and electrocatalytic performance of Pt NWs and Pt_3Ni NWs catalysts for ORR are investigated. The results show that Pt_3Ni NWs catalyst has a significantly higher electrocatalytic activity and a good stability for ORR as compared to Pt NWs and even Pt/C catalyst.

2 Experimental

2.1 Synthesis of catalysts

Pt and PtNi alloy nanowires catalysts were synthesized by using a soft template method [22]. In a typical synthesis for Pt_3Ni alloy nanowires catalyst, 4.24 mL of 23.6 mmol/L K_2PtCl_4 aqueous solution and 5 mL of 20 mmol/L $NiCl_2$ aqueous solution were mixed under vigorous stirring with 5 mL of chloroform solution containing 40 mmol/L of CTAB. For Pt nanowires catalyst, the steps were the same except the adjunction of Nickel precursor. Magnetic stirring was kept for 30 min to ensure the adequate transfer of Pt and Ni complex into the chloroform phase, followed by the addition of ultrapure water to make the whole volume equal to 80 mL. After stirring for another 30 min, 10 mL of ice-cold aqueous solution containing appropriate amount of $NaBH_4$ (0.4 g) was added to the above mixture under stirring for 30 min. The catalyst products were separated from the reaction system by centrifugation and cleaning with ultrapure water and ethanol for at least three times respectively. Then, XC-72 was dispersed in ethanol by ultrasonication for 30 min. The Pt or Pt_3Ni alloy nanowires catalyst dispersion in ethanol was mixed with the XC-72 suspension under vigorous stirring for 1 h to form Pt nanowires/C or Pt_3Ni alloy nanowires/C catalyst. The catalyst powder was collected by centrifugation and cleaning for three times and finally dried in a vacuum oven at 60°C for 12 h. The catalyst ink was prepared by ultrasonically mixing the catalyst with isopropyl alcohol (2 mg/mL) and Nafion (5% (wt.) in water) together.

2.2 Physical characterization

The crystal phase of the samples were measured by X-ray diffraction (XRD, BrukerD8, Cu Kα radiation). The morphology and structure of the samples was observed by using transmission electron microscope (TEM, JEM-2100) and high-resolution TEM (HRTEM) character was operated at 200 kV. The surface analysis and composition of the products were measured by using X-ray photoelectron spectroscopy (XPS, Thermo Scientific ESCALAB 250 Xi spectrometer, Al Kα in twin anode). The metals contents of the catalysts were detected by using inductive coupled plasma-optical emission spectroscopy (ICP-OES).

2.3 Electrochemical test

Electrochemical measurements were performed on a rotational disc electrode system (Pine) with a CHI730 workstation at room temperature in a conventional three-electrode cell with saturated calomel electrode (SCE) as the reference electrode and a Pt-foil as the counter electrode. Thin film of different catalysts on glass carbon electrode with the same Pt loading was used as the working electrode. N_2 and O_2-saturated 0.1 mol/L $HClO_4$ solution were used as the electrolyte for cyclic voltammetry and linear scanning voltammetry techniques respectively. The polarization curves for ORR was measured at a speed of 1600 r/min with a scan rate of 10 mV/s. The stability of different catalysts was measured by an accelerated deterioration test (ADT) procedure performed from 0.6 V to 1.0 V (vs. RHE) with a scan rate of 100 mV/s for 5000 cycles. The electrochemical specific surface area (ECSA) was calculated by integrating the areas of Pt-hydrogen region assuming 0.21 mC/cm^2 for the desorption charge of a monolayer of hydrogen atoms on a clean Pt surface [23]. The fabrication of Pt and PtNi alloy nanowires is schematic illustrated in Fig. 1.

3 Results and discussion

The high-crystallinity nature and bimetallic alloy characteristic of the as-prepared PtNi alloy NWs is confirmed by XRD first, as shown in Fig. 2. The diffraction peaks of (111), (200), (220) and (311) are easily to be indexed to face centered cubic (fcc) structured PtNi alloy (Pt, no. 04-0802 and Ni, no. 04-0850). When compared to pure Pt (Pt NWs and Pt/C), the diffraction peaks of PtNi alloy NWs shift slightly to higher 2θ values and bigger width, which could be attributed to the decrease of lattice distance when smaller Ni atoms replace Pt atoms in the lattice [24]. This geometric effect or strain effect resulted from the lattice contraction can weaken the strength of the Pt-O bond, i.e., can weaken the adsorption of intermediate oxygen

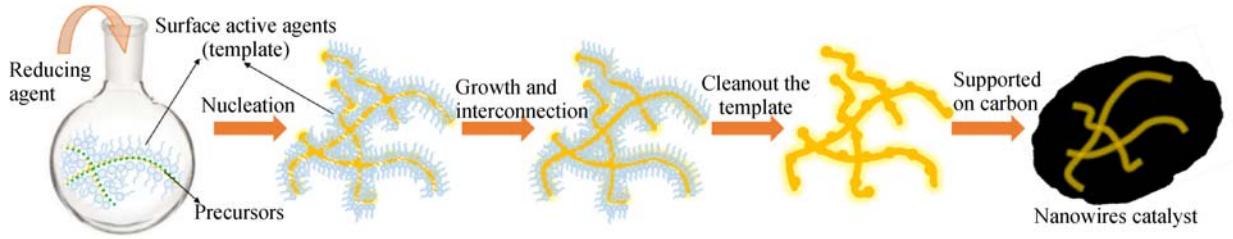

Fig. 1 Schematic illustration for the fabrication of Pt and PtNi alloy nanowires

containing species (O_{ads} or OH_{ads}), which beneficially improve the electrocatalytic activity [25,26]. In addition, it is worth noting that, compared to Pt/C catalyst, there are some high index diffraction peaks in Pt and PtNi alloy NWs, which may have also made contributions to the enhanced catalytic activity.

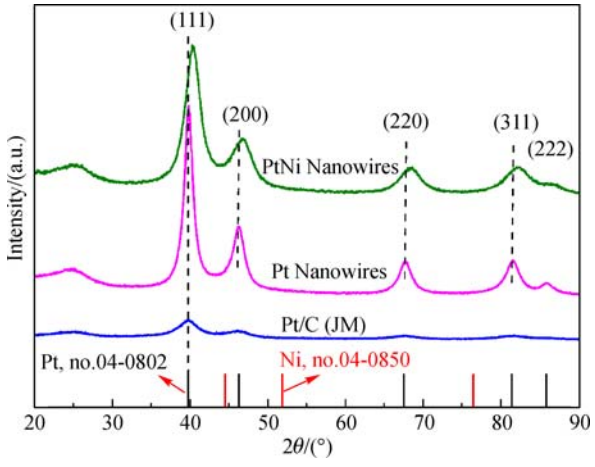

Fig. 2 XRD patterns of the commercial Pt/C catalyst (20% (wt.), JM) and the as-prepared Pt NWs and PtNi alloy NWs supported on XC-72

The composition of the PtNi alloy NWs was estimated using the shift of peaks from Vegard's law, $(1-x)a_1 + xa_2 = a$, with x being the molar fraction of the Ni; a_1, the lattice constant of the Pt (Reference code: 004-0802, 0.3923 nm); a_2, the lattice constant of the Ni (Reference code: 004-0850, 0.3524 nm); and a, the measured lattice constant of the formed PtNi alloy [27]. According to the position of the (111) peak after alloying with Ni and the Bragg equation, the lattice constant, a, and the lattice spacing d of the PtNi alloy NWs were calculated to be 0.3844 nm and 0.2219 nm, respectively. Thus the Pt/Ni composition of 79:21 was obtained with Vegard's law, by and large, in satisfactory agreement with the result detected by the EDS (average value of Pt/Ni = 76:24). In addition, there is no individual diffraction peaks of Ni in the XRD patterns, indicating that all or the majority of the Ni atoms enters the lattice of Pt to form alloy.

The morphology and nanowire-structure of the Pt NWs and Pt_3Ni alloy NWs were observed by using TEM and HRTEM, as illustrated in Fig. 3. As shown in Fig. 3(a) and (d), superficially, the products prepared by using this soft template method have the appearance of nanowires or nanowire networks. The average diameters of Pt NWs and Pt_3Ni alloy NWs were calculated to be 2.2 nm and 2.4 nm, respectively, by statistical analysis. As is known to all, for catalytic reaction, the specific surface area of the catalyst materials has an important influence on the activity. From this point of view, although the catalysts synthesized here form nanowires rather than nanoparticles, the ultrathin diameter ensures the sufficient surface area and platium utilization. Figure 3(c) and (f) show that the nanowire is composed of interconnected particles with a large number of grain boundaries, the existence of which is proven to be beneficial to improve the catalytic activity [22]. Further insights into the morphology and structure of the Pt and Pt_3Ni alloy NWs obtained from HRTEM observation are demonstrated in Fig. 3(c) and (f). The lattice spacing of Pt_3Ni alloy NWs is measured to be 0.22 nm, in satisfactory agreement with the value calculated by the XRD shift, a little smaller than that of the pure Pt(111) planes (0.23 nm), which also indicates the successful incorporation of Ni atoms into the Pt crystal structure. As mentioned earlier, this lattice contraction in PtNi alloy, to some extent, can enhance the electrocatalytic activity for ORR.

The composition of the Pt_3Ni alloy NWs and the electronic structure of Pt were investigated by the using XPS. The most intense peak of Pt $4f_{7/2}$ is assigned to metallic Pt (0) and the second peak is assigned to Pt (II). Notably, the Pt 4f binding energy of Pt_3Ni alloy NWs is blue-shifted compared to that of Pt NWs. The positions of Pt $4f_{7/2}$ are 71.11 and 71.31 eV for Pt NWs and Pt_3Ni alloy NWs, respectively (shown in Fig. 4(b) and 4(d)). The slight shift to higher binding energies may be attributed to a significant attribution from the interaction between Pt and Ni, an electron-withdrawing effect of Pt from the neighboring Ni atoms due to the different electronegativity of Pt and Ni (2.28 and 1.91). The binding energy strongly influences the adsorption/desorption capability of reaction species on the catalyst surface. Such a trend caused by the interactions between Pt and Ni indicates that the d-band center of Pt_3Ni alloy NWs catalyst downshifts compared to that of pure Pt NWs, which is beneficial to improve the

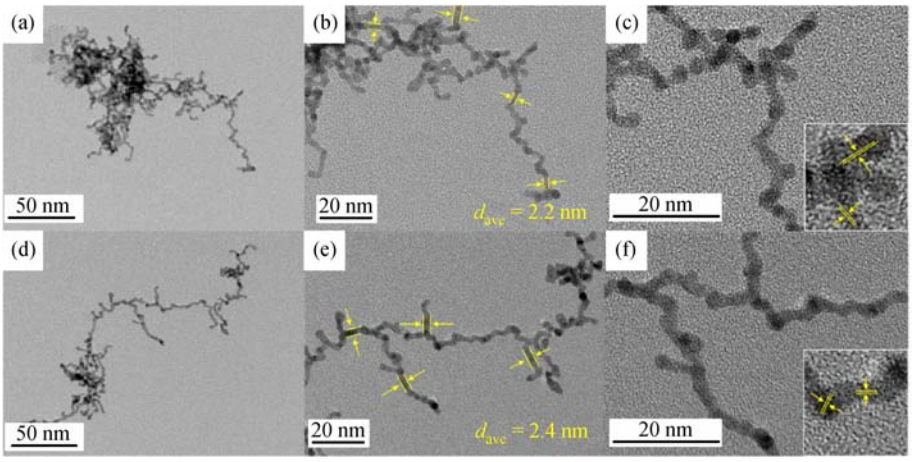

Fig. 3 Representative TEM and HRTEM images
(a), (b), (c) Synthetic Pt NWs; (d), (e), (f) PtNi alloy NWs

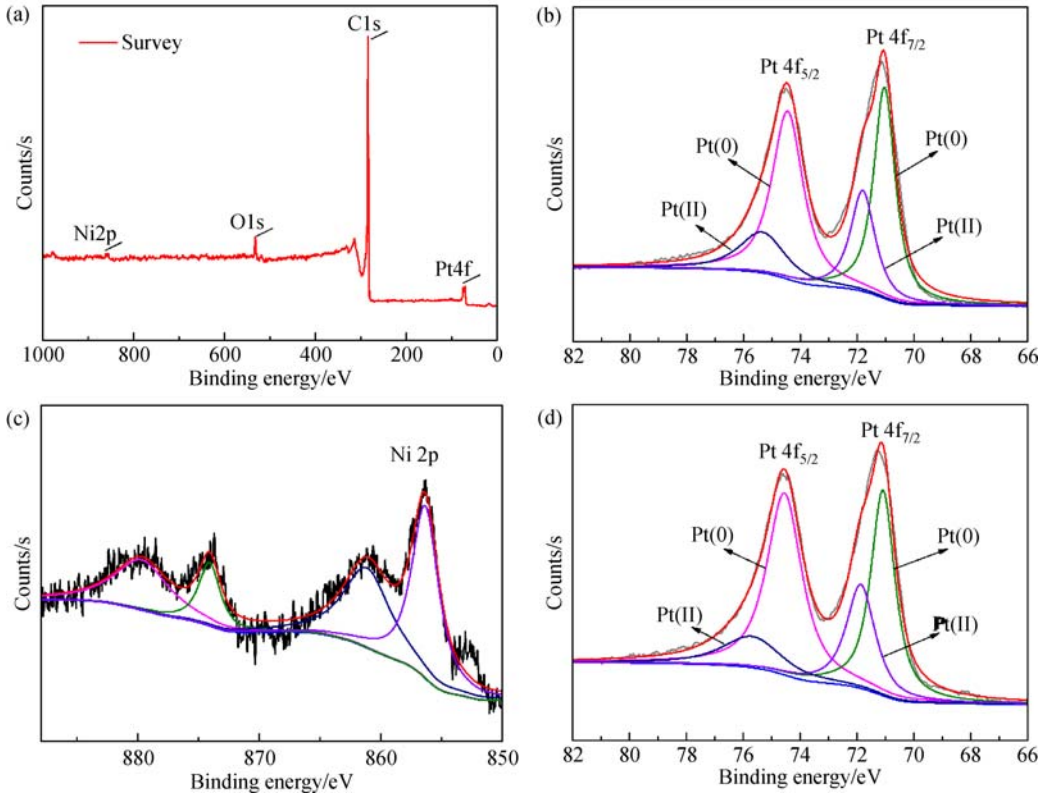

Fig. 4 XPS spectra
(a), (c), (d) The survey, Ni2p, and Pt4f for PtNi alloy NWs; (b) the Pt4f for Pt NWs

catalytic activity [28]. Additionally, the proportion of Pt in the metallic state of Pt_3Ni alloy NWs is higher than that of Pt NWs, which indicates higher utilization of Pt and maybe also better electrocatalytic performance of the Pt_3Ni for ORR.

The electrocatalytic performance of the as-prepared Pt and Pt_3Ni alloy NWs catalysts for ORR, compared with the commercial Pt/C catalyst, was evaluated by the half-cell test and the results are shown in Fig. 5. CVs of Pt and Pt_3Ni alloy NWs (Fig. 5(a)) show typical Pt-like H under potential deposition features but relatively smaller adsorption and desorption areas than Pt/C. After calculation, the electrochemical surface area of Pt/C, Pt NWs and Pt_3Ni alloy NWs are 80.3 m^2/g, 58.1 m^2/g, and 64.8 m^2/g.

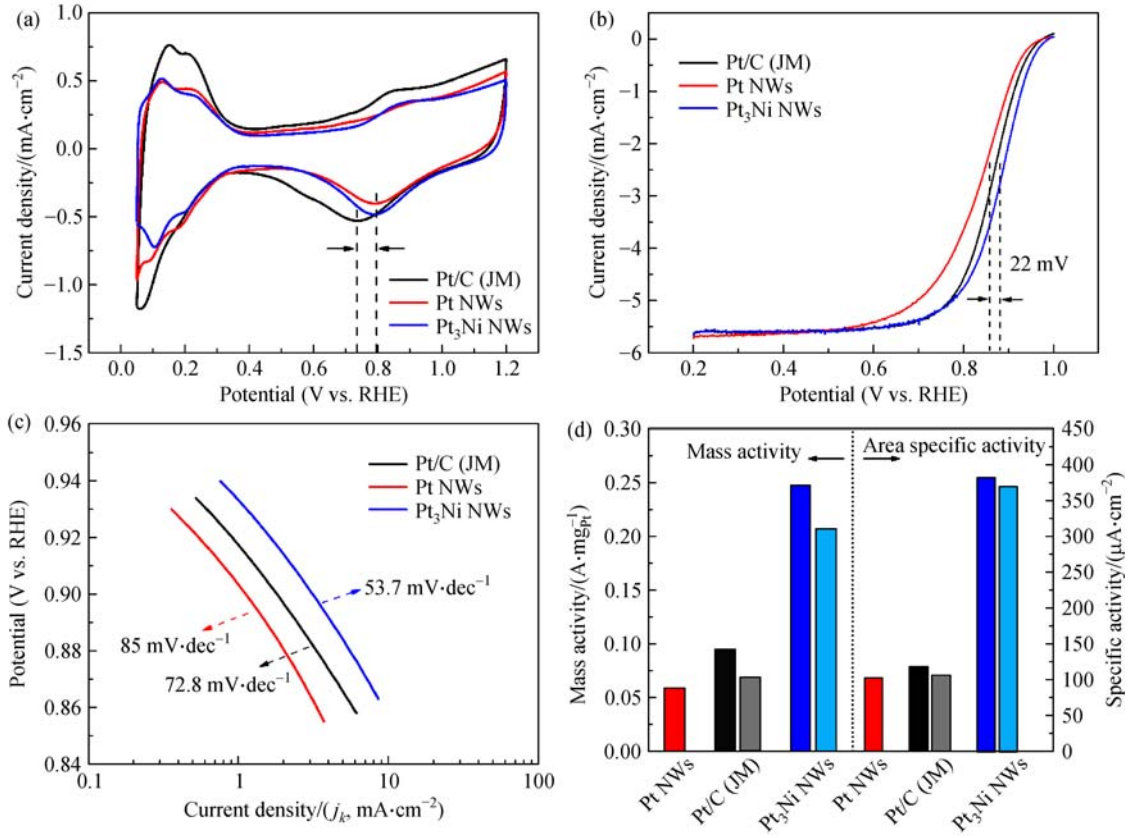

Fig. 5 RDE electrochemical characterization in 0.1 mol/L $HClO_4$ of commercial Pt/C catalyst compared to the as-prepared Pt NWs and the PtNi alloy NWs catalysts

(a) Cyclic voltammetry in argon-purged electrolyte; (b) polarization curves for the ORR; (c) corresponding Tafel plots of the catalysts; (d) summary of the SA and MA for the ORR at 0.9 V (vs. RHE) before (deep color) and after (light color) the same ADT process

Although the as-prepared Pt and Pt_3Ni alloy NWs catalysts show a smaller ECSA due to the structural reasons, the reduction peaks of which (~0.795 V vs. RHE) in the cathodic scan have an obvious positive shift compared to that of Pt/C catalyst (Fig. 5(a), ~0.736 V vs. RHE). Moreover, compared to Pt NWs, the Pt_3Ni alloy NWs has a higher current density at the reduction peak despite a little higher oxidation current density for Pt NWs. The positive shift and bigger reduction in current density of Pt_3Ni alloy NWs can be attributed to the reduced adsorption strength of intermediate oxygen containing species (O_{ads} or OH_{ads}) on the alloy surface, and more fundamentally, due to the downshift of the d band center as a result of the electronic effect and the strain effect in Pt_3Ni alloy. Pt is the best catalyst among the known single-metal catalysts for ORR but it is not exactly at the top of the "volcano curve" because of a bit stronger bonding between Pt and O_{ads} or OH_{ads}. The reduced surface coverage of oxides via the lease of active sites due to reduced adsorption strength led to a substantial enhancement in the ORR catalytic activity for Pt_3Ni alloy NWs catalyst, just as evidenced by the positive shift (22 mV) of half wave potential compared to Pt/C catalyst in the polarization curves (Fig. 5(b)). In addition, the ORR onset potential of Pt_3Ni alloy NWs catalyst attains 0.99 V (vs. RHE), which is ~15 mV higher than that of Pt/C catalyst, suggesting excellent ORR activity of the Pt_3Ni alloy NWs, too. Moreover, the Tafelslope of Pt/C catalyst and the prepared Pt and PtNi alloy NWs catalysts with respect to the ORR reaction mechanism was discussed. As shown in Fig. 5(c), the Tafel slop of Pt_3Ni alloy NWs (53.7 mV/dec) is smaller than that of both Pt/C (72.8 mV/dec) and Pt NWs.

The considerably smaller slope achieved in the Pt_3Ni alloy NWs catalyst suggests significantly improved kinetics for ORR. The area specific activity (ASA) and the mass activity (MA) were normalized by the ECSA and the total Pt loading, respectively. Specifically, the Pt_3Ni alloy NWs catalyst showed an ASA of 382.9 μA/cm^2, 3.7 times higher than that of Pt NWs (102.5 μA/cm^2) and 3.2 times higher than that of Pt/C (118.7 μA/cm^2) and a MA of 0.25 A/mg, 4.2 times higher than that of Pt NWs (0.059 A/mg) and 2.6 times higher than that of Pt/C (0.095 A/mg) at 0.90 V versus RHE tested under the same conditions.

The durability of the Pt_3Ni alloy NWs catalyst and the

Pt/C catalyst was evaluated using an ADT procedure. The base CVs and ORR polarization curves of the Pt_3Ni alloy NWs catalyst and the Pt/C catalyst before and after ADT are depicted in Fig. 6. The as-prepared Pt_3Ni alloy NWs catalyst shows good stability with smaller decline of the ECSA and few decrease of the half-wave potential. After 5000 cycles, the ECSA of Pt/C dropped by ~18.75%. In contrast, there is a ~13.67% decrease in the ECSA of the Pt_3Ni alloy NWs under the same ADT condition. For Pt/C catalyst, the MA and the half-wave potential after ADT drops by 31.6% and 14 mV, respectively, however, for the Pt_3Ni alloy NWs catalyst, the MA and the half-wave potential only drops by 16.4% and 9 mV. In addition, there is a problem to be considered for alloy catalysts that the dissolution of transition metal elements may do harm to other parts of the PEMFC, such as membranes. Therefore, the stability of the catalyst, especially the durability of the alloy material itself under the fuel cell operating conditions, is very important. Here, the loss rate of Ni during the ADT process was measured to be 25.96 %, to some extent, explaining the stability of this alloy nanowire catalyst with inherent structural stability. To achieve a better stability, the dissolution rate of Ni can be further reduced, for example, by the protection of Pt skin or the addition of other corrosion resistant metals. The ASA and MA before and after 5000 cycles ADT for Pt/C catalyst and the Pt_3Ni alloy NWs catalyst are summarized in Fig. 5(d). During the ADT procedure with periodically changed potential, Pt nanoparticles suffered from dissolution, agglomeration and Ostwald ripening which caused a considerable decrease of ECSA and the catalytic activity. The corrosion of carbon support under the operational conditions of PEMFC and the consequent abscission of Pt nanoparticles are also important factors resulting in poor stability. However, for the Pt_3Ni alloy NWs prepared here, the inherent structural stability of the unique nanowire or nanowires network structure can deter the transfer, agglomeration and Ostwaldripening process. The Pt_3Ni alloy NWs has multiple anchoring points and their mobility is much lower compared to particles with a single point contact on carbon support, weakening the influence of support corrosion. Above factors together contribute to the good stability of the Pt_3Ni alloy NWs catalyst.

4 Conclusions

In summary, PtNi alloy NWs catalyst with a controlled composition of 3:1 for Pt:Ni was synthesized by using a soft template method. The Pt_3Ni alloy NWs is composed of

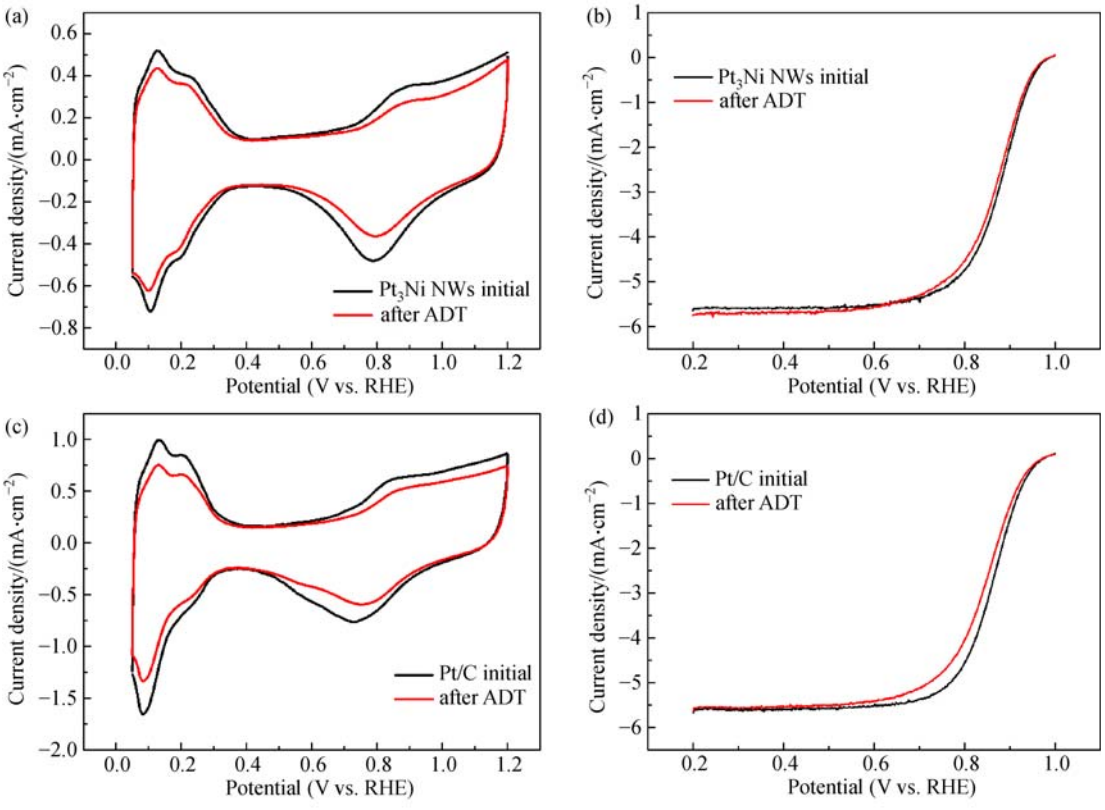

Fig. 6 Cyclic voltammograms with a scan rate of 50 mV/s and the ORR polarization curves (a), (b) PtNi alloy NWs; (c), (d) PtC catalyst before and after ADT (85.0 mV/dec)

interconnected nanoparticles with a large number of grain boundaries. The as-prepared Pt_3Ni alloy NWs catalyst shows enhanced electrocatalytic activity for ORR than Pt NWs and even the commercial Pt/C catalyst. The enhancement of activity can be mainly attributed to the reduced adsorption strength of intermediate oxygen containing species on the catalyst surface as a result of the electronic effect and the strain effect. The unique structure of nanowires or nanowire networks and multi-point contact with carbon support for Pt_3Ni alloy NWs catalyst make it exhibit good stability. The developed ultrathin-nanowire catalyst of Pt or Pt-based alloy is indeed a promising electrocatalyst for ORR in PEMFC.

Acknowledgements This work is financially supported by The National Key Research and Development Program of China (Grant No. 2016YFB0101208) and National Natural Science Foundation of China (Grant No.U1508202 and No.61433013).

References

1. Debe M K. Electrocatalyst approaches and challenges for automotive fuel cells. Nature, 2012, 486(7401): 43–51
2. Tang Q, Jiang L, Jiang Q, Wang S, Sun G. Enhanced activity and stability of a Au decorated Pt/PdCo/C electrocatalyst toward oxygen reduction reaction. Electrochimica Acta, 2012, 77(9): 104–110
3. Bele M, Jovanovic P, Pavlisic A, Jozinovic B, Zorko M, Recnik A, Chernyshova E, Hocevar S, Hodnik N, Gaberscek M. A highly active $PtCu_3$ intermetallic core-shell, multilayered Pt-skin, carbon embedded electrocatalyst produced by a scale-up sol-gel synthesis. Chemical Communications, 2014, 50(86): 13124–13126
4. Zhang J, Sasaki K, Sutter E, Adzic R R. Stabilization of platinum oxygen-reduction electrocatalysts using gold clusters. Science, 2007, 315(5809): 220–222
5. Wang Y J, Zhao N N, Fang B Z, Li H, Bi X T T, Wang H J. Carbon-supported Pt-based alloy electrocatalysts for the oxygen reduction reaction in polymer electrolyte membrane fuel cells: particle size, shape, and composition manipulation and their impact to activity. Chemical Reviews, 2015, 115(9): 3433–3467
6. Chen Z W, Higgins D, Yu A P, Zhang L, Zhang J J. A review on non-precious metal electrocatalysts for PEM fuel cells. Energy & Environmental Science, 2011, 4(9): 3167–3192
7. Zheng Y, Jiao Y, Jaroniec M, Jin Y G, Qiao S Z. Nanostructured metal-free electrochemical catalysts for highly efficient oxygen reduction. Small, 2012, 8(23): 3550–3566
8. Bai Y Z, Yi B L, Li J, Jiang S F, Zhang H J, Shao Z G, Song Y J. A high performance non-noble metal electrocatalyst for the oxygen reduction reaction derived from a metal organic framework. Chinese Journal of Catalysis, 2016, 37(7): 1127–1133
9. Greeley J, Mavrikakis M. Alloy catalysts designed from first principles. Nature Materials, 2004, 3(11): 810–815
10. Wu J B, Yang H. Platinum-based oxygen reduction electrocatalysts. Accounts of Chemical Research, 2013, 46(8): 1848–1857
11. Zhang J, Mo Y, Vukmirovic M B, Klie R, Sasaki K, Adzic R R. Platinum monolayer electrocatalysts for O_2 reduction: Pt monolayer on Pd(111) and on carbon-supported Pd nanoparticles. Journal of Physical Chemistry B Materials Surfaces Interfaces Amp Biophysical, 2004, 108(30): 10955–10964
12. Zhang J L, Vukmirovic M B, Xu Y, Mavrikakis M, Adzic R R. Controlling the catalytic activity of platinum-monolayer electrocatalysts for oxygen reduction with different substrates. Angewandte Chemie, 2005, 44(14): 2132–2135
13. Zhu H Y, Zhang S, Guo S J, Su D, Sun S H. Synthetic control of FePtM nanorods (M = Cu, Ni) to enhance the oxygen reduction reaction. Journal of the American Chemical Society, 2013, 135(19): 7130–7133
14. You H J, Yang S C, Ding B J, Yang H. Synthesis of colloidal metal and metal alloy nanoparticles for electrochemical energy applications. ChemInform, 2013, 42(7): 2880–2904
15. Zhao X, Yin M, Ma L, Liang L, Liu C P, Liao J H, Lu T H, Xing W. Recent advances in catalysts for direct methanol fuel cells. Energy & Environmental Science, 2011, 4(8): 2736–2753
16. Li Y J, Chen L, Chen K, Quan F X, Chen C F. Monodisperse PdCu@PtCu Core@Shell nanocrystal and their high activity and durability for oxygen reduction reaction. Electrochimica Acta, 2016, 192: 227–233
17. Wang G, Huang B, Xiao L, Ren Z, Chen H, Wang D, Abruña H D, Lu J, Zhuang L. Pt skin on AuCu intermetallic substrate: a strategy to maximize Pt utilization for fuel cells. Journal of the American Chemical Society, 2014, 136(27): 9643–9649
18. Huang X Q, Zhao Z P, Chen Y, Zhu E B, Li M F, Duan X F, Huang Y. A rational design of carbon-supported dispersive Pt-based octahedra as efficient oxygen reduction reaction catalysts. Energy & Environmental Science, 2014, 7(9): 2957–2962
19. Huang X Q, Zhao Z P, Cao L, Chen Y, Zhu E B, Lin Z Y, Li M F, Yan A M, Zettl A, Wang Y M, Duan X F, Mueller T, Huang Y. High-performance transition metal-doped Pt_3Ni octahedra for oxygen reduction reaction. Science, 2015, 348(6240): 1230–1234
20. Chen C, Kang Y J, Huo Z Y, Zhu Z W, Huang W Y, Xin H L L, Snyder J D, Li D G, Herron J A, Mavrikakis M, Chi M F, More K L, Li Y D, Markovic N M, Somorjai G A, Yang P D, Stamenkovic V R. Highly crystalline multimetallic nanoframes with three-dimensional electrocatalytic surfaces. Science, 2014, 343(6177): 1339–1343
21. Yang H Z, Zhang J, Sun K, Zou S Z, Fang J Y. Enhancing by weakening: electrooxidation of methanol on Pt_3Co and Pt nanocubes. Angewandte Chemie International Edition in English, 2010, 49(38): 6848–6851
22. Wang S Y, Jiang S P, Wang X, Guo J. Enhanced electrochemical activity of Pt nanowire network electrocatalysts for methanol oxidation reaction of fuel cells. Electrochimica Acta, 2011, 56(3): 1563–1569
23. Pozio A, de Francesco M, Cemmi A, Cardellini F, Giorgi L. Comparison of high surface Pt/C catalysts by cyclic voltammetry. Journal of Power Sources, 2002, 105(1): 13–19
24. Stamenkovic V R, Fowler B, Mun B S, Wang G F, Ross P N, Lucas C A, Markovic N M. Improved oxygen reduction activity on Pt_3Ni (111) via increased surface site availability. Science, 2007, 315 (5811): 493–497
25. Bu L Z, Zhang N, Guo S J, Zhang X, Li J, Yao J L, Wu T, Lu G, Ma J Y, Su D, Huang X Q. Biaxially strained PtPb/Pt core/shell nanoplate boosts oxygen reduction catalysis. Science, 2016, 354

(6318): 1410–1414

26. Suo Y G, Zhuang L, Lu J T. First-principles considerations in the design of Pd-alloy catalysts for oxygen reduction. Angewandte Chemie, 2007, 46(16): 2862–2864
27. Jayasayee K, van Veen J A R, Manivasagam T G, Celebi S, Hensen E J M, de Bruijn F A. Oxygen reduction reaction (ORR) activity and durability of carbon supported PtM (Co, Ni, Cu) alloys: influence of particle size and non-noble metals. Applied Catalysis B: Environmental, 2012, 111–112(2): 515–526
28. Wang D S, Li Y D. Bimetallic nanocrystals: liquid-phase synthesis and catalytic applications. Advanced Materials, 2011, 23(9): 1044–1060